[American Journal of Science, Vol. 314, March, 2014, P. 785–804, DOI 10.2475/03.2014.02]

WATER-ROCK INTERACTION AND REACTIVE-TRANSPORT MODELING USING ELEMENTAL MASS-BALANCE APPROACH: I. THE METHODOLOGY

ANTHONY J. PARK

Sienna Geodynamics and Consulting, Inc., 101 Kirkwood Avenue, Suite 222, Bloomington, Indiana 47404; ajpark@sienna-geo.com; (781) 534-5134

ABSTRACT. Water-rock interaction and reactive transport modeling is an important tool for deciphering chemical and physical reactions occurring in sediments and rocks. The modeling methodology calls for solving conservation equations to account for the interaction between mass-transfer and reaction processes using a sequential iteration numerical method.

The formalism presented here improves upon the traditional approach by reformulating conservation equations to express chemical elemental mass evolution. The elemental conservation equations describe mass change through mass-transfer and kinetic reactions of solids, and solute-solute interaction (equilibrium) reaction expressions. The system of equations is solved using a sequential iteration method, whereby globally discretized mass-transfer coefficients of conservation equations are injected explicitly into the conservation equations and solved locally at each node. The result is a mathematically simple approach that eliminates the traditionally required use of primary and secondary species classification. The formalism also allows the use of solute-specific diffusivities. In addition, the tight coupling between mass-transfer and reactions achieved by the methodology also allows nonlinear self-organization or pattern-forming phenomena to be captured.

The methodology is demonstrated with simulations of (1) a diffusive-reaction system involving patterned hematite nucleation, and (2) a flow-through system where CO_2-charged water interacts with formation water in a sandstone reservoir. Both are isothermal one-dimensional simulations. In the first example, convergent diffusive infiltration of Fe^{++} and O_2 from two opposite ends produces patterned precipitates. A natural analog of such phenomena is the occurrence of iron-oxide concretions in Navajo Sandstones of Utah and Arizona. The second example demonstrates the formation of a diffusive solute migration front ahead of advective effluent displacement and reaction fronts. Such phenomena are observed when large quantities of CO_2 are injected into geologic formations. The early arrival of diffusive solute fronts at nearby monitoring wells are noted by decreasing water pH and raised alkalinity some time before the arrival of the effluent.

Key words: Water-rock interaction, reactive-transport modeling, coupled nonlinear processes, rtm, kinetic reaction, rate law, liesegang process, reaction-diffusion system, iron-oxide concretion, nucleation, pattern-forming, self-organization, carbon sequestration, advective and diffusive mass-transfer

INTRODUCTION

Water-rock interaction models can be grouped generally into two types: closed-system or open-system. Closed-system models resolve water-rock interaction by solving chemical equilibrium reactions with or without kinetic reactions (Truesdell and Jones, 1974; Perkins and others, 1988; Wolery and others, 1990; Parkhurst and others, 1990). Inherently these models do not resolve diffusive or advective mass-transfer mechanisms in mathematically or phenomenologically self-consistent manner. Open-system water-rock interaction models address coupled mass-transfer and chemical (both equilibrium and kinetic) reactions of one or more minerals (Lichtner, 1985; White and Chuma, 1986; Ortoleva and others, 1987; Yeh and Tripathi, 1991; Steefel and Lasaga, 1994; Raffensperger and Garven, 1995; Boudreau, 1996; Xu and Pruess, 2001; Park and Ortoleva, 2003). The common trait of open-system models is that they solve a

set of mass-conservation equations that account for evolution of solute species concentrations associated with mass-transfer and reactions.

The continuum-based open-system models typically solve the solute mass-conservation equations by delineating primary and secondary solutes involving homogeneous (solute-solute) and heterogeneous (mineral-solute) reactions (Rubin, 1983; Lichtner, 1985; Steefel and Lasaga, 1994). By convention a primary solute is a compound that represents the total concentration of a particular chemical element, whereas a secondary solute is a linear combination of a number of primary solutes. Comprehensive but summary reviews of this (henceforth called the "conventional") approach and its background and development history can be found in Lichtner (1985), Kirkner and Reeves (1988), and Steefel and Lasaga (1994). Other works that present similar or modified versions of the same approach can be found in Yeh and Tripathi (1991), Raffensperger and Graven (1995), and Xu and Pruess (2001).

The continuum-based models use sequential iteration numerical methods that solve water flow, mass-transfer, and chemical interaction processes separately (Lichtner, 1985; Kirkner and Reeves, 1988; Yeh and Tripathi, 1991; Steefel and Lasaga, 1994; Raffensperger and Garven, 1995; Xu and Pruess, 2001; Park and Ortoleva, 2003). However, no formal methodology has been proposed for the implementation of the sequential iteration method, and each model tends to use its own unique method of addressing the coupling between mass-transfer and chemical interaction.

As an alternative to the conventional continuum-based water-rock interaction models, a methodology is presented here that solves elemental mass conservation equations. This is in contrast to the conventional methods that use solute mass conservation equations, and offers a number of important advantages. Primarily, it provides a mathematically simpler and well-defined method of constructing a system of equations for solving water-rock interaction and mass-transfer processes. Distinctions of primary and secondary species therefore become unnecessary.

The methodology is complemented by a discretization approach that clearly shows mathematically self-consistent sequential iteration between mass-transfer and reactions. The discretization method can be used with any one of the popular numerical methods (finite difference, finite volume, and others). Altogether, the methodology presented in this paper makes it possible to achieve near-exact conservation (at the limit of numerical method and round-off errors) of total mass of chemical elements through diffusive and advective mass-transfer processes, equilibrium reactions among solutes, and kinetic reactions between solutes and minerals.

The utility of the methodology is demonstrated through two simulation examples consisting of 1) Liesegang-type reaction-diffusion system describing iron-oxide precipitation, and 2) one-dimensional reactive-flow problem that occurs between injected CO_2 and formation water in a saline reservoir. To simplify the illustrations of the method, heat transfer and variable flux are ignored by using constant-temperature and constant-flux or no-flux conditions.

CONSERVATION EQUATIONS

The standard form of conservation of mass, formulated for keeping track of solute species mass in pore water due to mass-transfer and reactions, is written as (deGroot and Mazur, 1962)

$$\phi \frac{\partial c_\alpha}{\partial t} = \phi D_\alpha \nabla^2 c_\alpha - \phi \vec{\nabla} \cdot (c_\alpha \vec{u}) - \sum_{\gamma=1}^{M} \nu_{\alpha\gamma} A_\gamma G_\gamma \qquad (1)$$

for porosity ϕ, solute species index α, solute molar concentration c_α, diffusion coefficient D_α (cm^2/sec), water flow (Darcy) velocity $\vec{u}$ (cm/sec), mineral index γ,

stoichiometry of solute α in the γ-th kinetic reaction $\nu_{\alpha\gamma}$, mineral surface area A_γ ($/cm^2$), and mineral (kinetic) reaction rate G_γ (moles/cm^2-sec). In order, the first two terms on the right-hand-side of equation (1) describe diffusive and advective fluxes, respectively, and the third term identifies contributions due to reactions. More detailed description of G_γ and the rate law is given in a following section. In this formulation, porosity is assumed constant. The case involving variable porosity and porous media composition will be addressed separately in another manuscript.

Equation (1) is a solute conservation equation that shows a solute concentration evolution dependence on mass-transfer and chemical reactions. However, the reaction-term of the equation (1) should be reconsidered in the form

$$\phi \frac{\partial c_\alpha}{\partial t} = \phi D_\alpha \nabla^2 c_\alpha - \phi \vec{\nabla} \cdot (c_\alpha \vec{u}) - \sum_{\eta=1}^{Nf} \nu_{\alpha\eta} F_\eta - \sum_{\gamma=1}^{M} \nu_{\alpha\gamma} A_\gamma G_\gamma \tag{2}$$

where Nf and F_η denote the number of reactions that involve solute species only and their respective reaction rates, respectively (Ortoleva and others, 1987). This formalism assumes that in most geologic systems mineral reaction rates are significantly slower than the rates of reactions involving only solute species. As in the conventional continuum-based models (Rubin, 1983; Lichtner, 1985; Yeh and Tripathi, 1991; Steefel and Lasaga, 1994; Park and Ortoleva, 2003), the Nf number of reactions can be assumed to be "fast" according to these authors, and also described using equilibrium reactions rather than kinetic reaction rate laws. These "fast" equilibrium solute-solute reactions are expressed mathematically as

$$\prod_{\alpha=1}^{Na} a_\alpha^{\nu_{\alpha\eta}} = K_\eta \tag{3}$$

for activity of the α-th solute a_α, stoichiometry of the solute in the η-th reaction $\nu_{\alpha\eta}$, equilibrium constant of the reaction K_η, in a system consisting of Na number of solute species. The activity of the solute α is typically calculated through the relationship

$$a_\alpha = \gamma_\alpha m_\alpha \tag{4}$$

where m_α is the molal concentration of solute α, and γ_α is the activity coefficient, which can be calculated using one of several available methods. The standard solute activity correction method assumed in this manuscript is the extended Debye-Huckel (b-dot) model (Wolery and others, 1990; Wolery, 1992).

Because the waters used in the example simulations are dilute and its mass density change associated with reactions is negligible, molar and molal quantities are used interchangeably in the methodology presented here. Otherwise, conversion between molal (moles/kg of water) and molar (moles/liter of solution) concentrations can be accomplished by using the water mass density to calculate equivalent volume of solution. However, it must be noted that the molar-molal conversion using water density alone is an imprecise methodology, if the water composition is changing. This is because changing solute concentrations can modify the solution volume due to the effects associated with partial molar volumes of solutes (Millero, 1971).

The solute mass-conservation equation can be reformulated to conserve chemical elements. This approach makes use of the fact that the total mass of an element in pore water is equal to the sum of the element in all of the solutes,

$$e_\beta = \sum_{\alpha=1}^{Na} \nu_{\beta\alpha} \phi c_\alpha \tag{5}$$

where e_β is the quantity of element β and $\nu_{\beta\alpha}$ is the stoichiometry of element β in aqueous species α. By combining equations (2) and (5), evolution of elemental mass in the water, per unit volume of porous media, is written as

$$\frac{\partial e_\beta}{\partial t} = \sum_{\alpha=1}^{Na} \nu_{\beta\alpha}\phi \frac{\partial c_\alpha}{\partial t}$$
$$= \sum_{\alpha=1}^{Na} \nu_{\beta\alpha}\left[\phi D_\alpha \nabla^2 c_\alpha - \phi\vec{\nabla}\cdot(c_\alpha\vec{u}) - \sum_{\eta=1}^{Nf} \nu_{\alpha\eta}F_\eta - \sum_{\gamma=1}^{M} \nu_{\alpha\gamma}A_\gamma G_\gamma\right]. \quad (6)$$

This transformation produces *Ne* number of elemental mass-conservation equations from *Na* number of solute mass-conservation equations.

Elemental mass is neither lost nor created through the *Nf* number of fast reactions. Therefore, the net change of an elemental mass through the fast reactions is zero, and equation (6) simplifies to

$$\frac{\partial e_\beta}{\partial t} = \sum_{\alpha=1}^{Na} \nu_{\beta\alpha}\left[\phi D_\alpha \nabla^2 c_\alpha - \phi\vec{\nabla}\cdot(c_\alpha\vec{u}) - \sum_{\gamma=1}^{M} \nu_{\alpha\gamma}A_\gamma G_\gamma\right]. \quad (7)$$

Separating out the reaction term from the mass-transfer terms, and recognizing that the dot product of the two stoichiometric matrices formed by elements in solutes $\nu_{\beta\alpha}$ and solutes in minerals $\nu_{\alpha\gamma}$ produces a stoichiometric matrix describing elements in minerals $\nu_{\beta\gamma}$, equation (7) is further simplified to

$$\frac{\partial e_\beta}{\partial t} = \sum_{\alpha=1}^{Na} \nu_{\beta\alpha}[\phi D_\alpha \nabla^2 c_\alpha - \phi\vec{\nabla}\cdot(c_\alpha\vec{u})] - \sum_{\gamma=1}^{M} \nu_{\beta\gamma}A_\gamma G_\gamma. \quad (8)$$

Note in particular, that even as the conservation equations have been rewritten to account for chemical elemental mass evolution, these equations are to be used to solve *Na* number of aqueous solute species concentrations. Therefore, to solve the water-rock interaction system consisting of *Na* number of solute species, one constructs *Na* number of equations using *Ne* number of elemental mass conservation equations (eq 8) and *Nf* number of fast reactions (eq 3). Furthermore, as the point is demonstrated in the examples, a geochemical problem consisting of *Na* number of solutes is constrained exactly by *Ne* number of elemental equations and *Nf* number of equilibrium reactions.

For a system consisting of *Na* number of solute species, the system of equations that consist of the same number of equations are solved using a numerical iterative method. To accomplish this, the *Ne* number of partial differential equations must be discretized for time and space. Presented in the following section is the procedure for discretizing and solving the system of equations using a Newton-Raphson iterative method.

DISCRETIZATION AND NUMERICAL METHOD

The sequential iterative scheme shown in figure 1 is a schematic representation of the numerical method used to construct a simulator that implements the methodology presented in this paper. Temperature distribution, water flow, water-rock interaction, and textural models are solved separately, but iterated within any given timestep to achieve convergence. The stiffness posed by the mass conservation equation requires that the water-rock interaction to be treated as a zero-dimensional problem, implying that the property of each computational node must be solved individually.

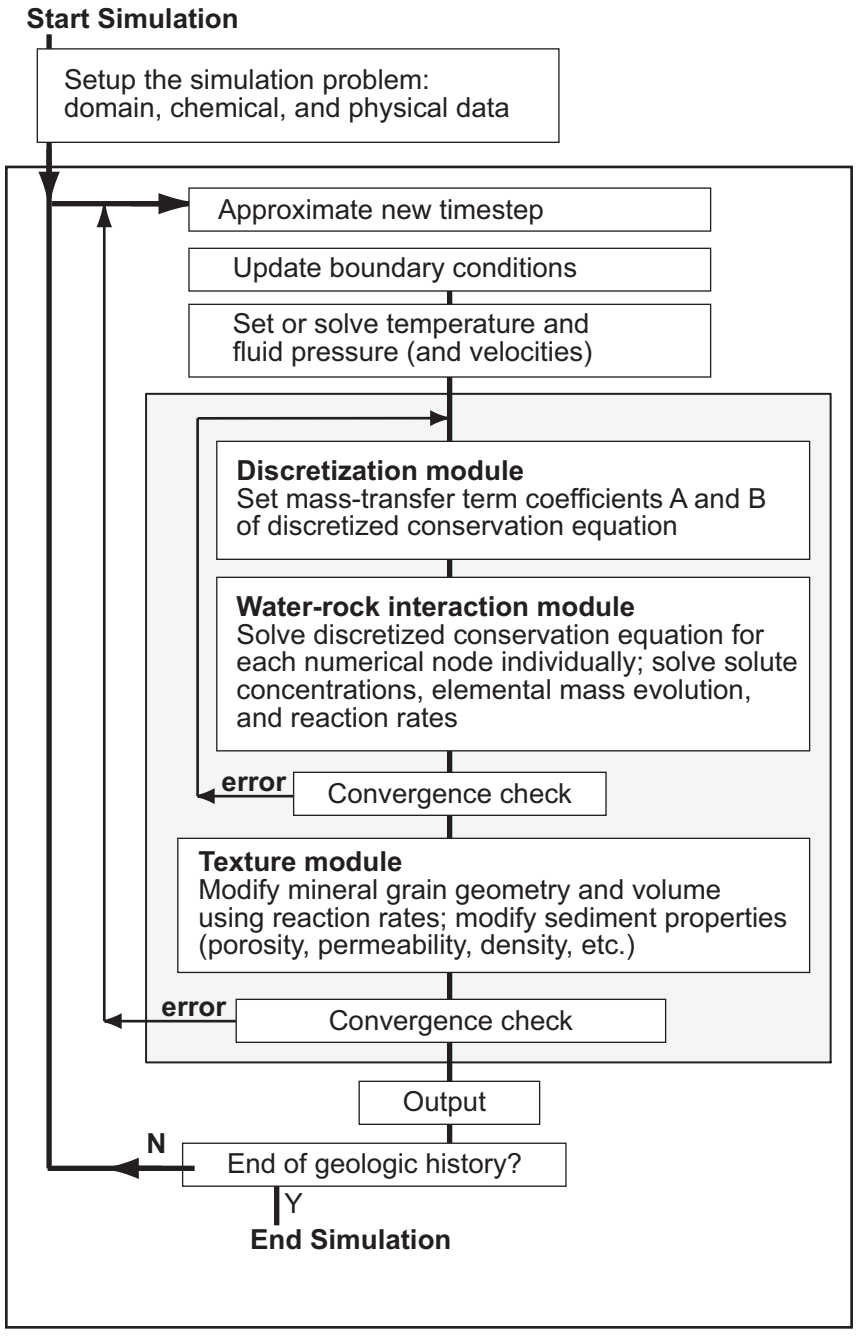

Fig. 1. Schematic diagram representing the iterative numerical method used to construct the forward time-stepping water-rock interaction and reactive-transport simulator used herein. (A) Hydrodynamics, water-rock interaction, and textural evolution are solved in separate modules or program functions for each timestep. The modules are solved iteratively until consistent solutions to all variables are achieved. (B) To preserve tight coupling between mass-transfer and reactions, water-flow velocities obtained from hydrodynamic module are used to form discretized mass-transfer coefficient matrices that are in turn used in the water-rock interaction module. Compositional and textural evolution is based on reaction rates calculated in the water-rock interaction module.

In this section a discritization that allows a precise formulation of mass-transfer contributions toward achieving solutions of the elemental mass-conservation equations is described. As shown in figure 1, fluid flow velocities, temperature, and other extrinsic properties must be resolved prior to invoking the water-rock interaction module. Subsequent to the water-rock interaction resolution, a textural model uses the mineral reaction rates obtained to modify texture and composition of minerals.

To preserve the tight coupling between mass-transfer and water-rock interaction, the elemental mass-conservation equation (7) is discretized in space and time as

$$e_\beta(t+\Delta t) - e_\beta(t)\big|_{i,j,k} = \Delta t\phi \sum_{\alpha=1}^{Na} \nu_{\beta\alpha}(A_\alpha\big|_{i\pm 1,j\pm 1,k\pm 1} + B_\alpha c_\alpha\big|_{i,j,k}) - \Delta t \sum_{\gamma=1}^{M} \nu_{\beta\gamma} A_\gamma G_\gamma \Bigg|_{i,j,k} \tag{9}$$

where A and B are constants produced from the discretization of diffusive and advective mass-transfer terms of the mass-conservation equation, and i, j, and k are indices of computational nodes along the x, y, and z axes, respectively. In this formulation coefficient A is a constant that describes the effects of solute concentrations of the neighboring nodes. Since each node is solved individually, this treatment is mathematically correct. By contrast, coefficient B describes the physical attributes of the node being solved. The effect of changing neighborhood node concentrations is incorporated into the system of equations by iterating the discretization and the water-rock interaction resolution modules as shown in figure 1. Thus, the iteration scheme consists of (1) obtaining A and B coefficients given fluid flow velocities, (2) solving the discretized elemental mass conservation equation (eq 8) along with equilibrium reaction expressions, and (3) iterating this sequence until the solution convergence criteria is achieved (fig. 1).

Coefficients A and B are obtained by writing out the discretized form of the conservation equation for the numerical method used to solve the system of equations, and gathering the parts of the mass-transfer terms that contain the concentration variable c. For example, when a one-dimensional regularly spaced finite difference method is used to solve the mass-conservation equation, the discretized mass-transfer term of equation (7) (using up-winding for positive flow rate) becomes

$$e_\beta(t+\Delta t) - e_\beta(t)\big|_i = \Delta t\phi \sum_{\alpha=1}^{Na} \nu_{\beta\alpha}\left(D_\alpha \frac{c_{\alpha,i+1} - 2c_{\alpha,i} - c_{\alpha,i-1}}{(\Delta x)^2} - u_x \frac{c_{\alpha,i} - c_{\alpha,i-1}}{\Delta x} \right) - \Delta t \sum_{\gamma=1}^{M} \nu_{\beta\gamma} A_\gamma G_\gamma \Bigg|_i \tag{10}$$

where Δx is the grid-spacing. Rearrangement of this equation produces $c_{\alpha,i}$ dependent and independent coefficients A and B, respectively, as

$$A_{\alpha,i} = D_\alpha \frac{c_{\alpha,i+1} - c_{\alpha,i-1}}{(\Delta x)^2} + u_{x,i} \frac{c_{\alpha,i-1}}{\Delta x} \tag{11}$$

$$B_{\alpha,i} = D_\alpha \frac{-2}{(\Delta x)^2} - u_{x,i} \frac{1}{\Delta x}. \tag{12}$$

Solute concentrations satisfying the elemental conservation (eq 7) and equilibrium conditions (eq 3) are achieved by solving Ne number of equations (8) and Nf

number of equilibrium reaction equations (3) simultaneously. This system of *Na* number of equations is solved using an iterative matrix solution approach, such as a Newton-Raphson method, combined with an efficient matrix reduction routine, such as Gauss-Jordan matrix reduction method with partial- or full-pivoting or LU decomposition (Atkinson, 1988; Press and others, 1992). The Newton-Raphson method can be expressed generally as

$$\underline{[c^{p+1}]} = \underline{[c^{p}]} - \underline{\underline{[f'(c^{p})]}}^{-1}\underline{[f(c^{p})]} \tag{13}$$

for the solute concentration variable c, numerical iteration counter p, and where two right-hand terms are residual (evaluated result of an equation) $f(c^p)$ and inverted Jacobian matrix of derivatives of the equations $f'(c^p)$. The single and double underlines indicate vectors and matrices with length *Na* and dimension (*Na* × *Na*), respectively. As solute concentrations are being solved, evolution of elemental masses are embedded in the residual terms. In effect, even as the water-rock interaction problem posed by equation (8) is to solve for evolving elemental mass, they are treated as constants in the numerical system that solves for solute concentrations. Thus, as concentration variables are solved according to the convergence criteria

$$err_c = max\left(\frac{c_\alpha^{p+1}}{c_\alpha^{p}} - 1\right) \leq 10^{-6} \tag{14}$$

elemental mass evolution is also resolved simultaneously to achieve

$$err_e \cong \min\left(\frac{e_\alpha^{p+1}}{e_\alpha^{p}} - 1\right) \leq 10^{-6}. \tag{15}$$

The convergence criteria are determined by trial and error.

Simulation timestep can be constrained at the beginning of each timestep iteration using the Courant-Friedrichs-Lewy condition (Courant and others, 1928) on flow velocity and diffusion rate limits,

$$\Delta t \leq \frac{\Delta x}{u_x} \qquad \text{and} \qquad \Delta t \leq \frac{(\Delta x)^2}{\max(D_\alpha)}, \tag{16}$$

as well as solute concentration evolution rate limit

$$\Delta t \leq \min\left(\frac{\Delta c_\alpha}{\nu_\alpha A_\gamma G_\gamma}\right) \tag{17}$$

for all solutes and corresponding reactions over all of the computational nodes. The goal here is to find the largest timestep that conforms to equations (16) and (17). The criteria of equation (16) are necessary for computational stability. Equation (17) is however more useful for avoiding oscillatory conditions from arising when one or more solute concentrations change too fast. Typically a solute concentration should not be allowed to change more than 5% within any given timestep.

KINETIC REACTION RATE LAW

The kinetic reaction-rate term G_γ of equations (1), (2), and (8) consists of two components: an Arrhenius temperature-dependent expression for reaction rate constant and a mass-action expression. A physico-chemical kinetic rate law can be written as

$$G_\gamma = k_{\gamma,diss}\left(\prod_{\substack{\alpha=1,\\ \nu_{\alpha\gamma}<0}}^{Na} a_\alpha^{-\nu_{\alpha\gamma}} \frac{1}{K_\gamma} \prod_{\substack{\alpha=1,\\ \nu_{\alpha\gamma}>0}}^{Na} a_\alpha^{\nu_{\alpha\gamma}}\right) \tag{18}$$

where $k_{\gamma,diss}$ and K_γ are dissolution rate constant and equilibrium constant of mineral γ, respectively. The quantity within the bracket is the mass-action component, with the first and the second product-multiple terms accounting for reactant and product species contributions, respectively. When water is supersaturated with respect to a mineral the value of G_γ becomes negative. The extent of saturation also determines the magnitude of the mass-action term.

The Arrhenius expression of the temperature dependence of the dissolution rate constant $k_{i,diss}$ in equation (18) is

$$k_{\gamma,diss} = k_{\gamma,o} \exp^{(-Ea_\gamma/RT)} \tag{19}$$

where $k_{\gamma,o}$ is the theoretical high-temperature limit of the dissolution rate constant, Ea_γ is the activation energy, and R and T are the gas constant and pore water temperature, respectively. The activation energy of the reaction describes a thermal threshold the reactants (molecules in the solid mineral state) must overcome to become products (solutes in the solvent) (Eyring, 1935).

Most reaction rate laws used in the geochemical literature are variants of the reaction rate law as written in equation (18), and reflect their adaptation to experimental and/or observational attributes. Such rate laws include, but are not limited to,

$$G_\gamma = k_{\gamma,diss}\left(1 - \frac{Q}{K_\gamma}\right) \tag{20}$$

$$G_\gamma = k_{\gamma,diss}[H^+]^n\left(1 - \frac{Q}{K_\gamma}\right) \tag{21}$$

where Q, often called the saturation quotient or ionic activity product (IAP), is equivalent to the second product-multiple term of equation (18). Equations (20) and (21) also assume that the water is sufficiently dilute and therefore first product-multiple term is unity. The value of n in equation (21) is empirically fit to experimental data and indicates the reaction rate dependence on the pH of the water. Rate laws (20) and (21) are equivalent to equation (18) when the solutions are dilute. Equation (20) and equation (21) are equivalent when the stoichiometry of H^+ is zero on the reactant side of a reaction. Therefore, a general rate law in the form of equation (18) allows more flexible and accurate treatment of chemical reactions between minerals and solutes.

DIFFUSION AND RELATED MASS-TRANSFER PROCESSES

Fick's first and second laws describe diffusive flux J_a of a solute species due to concentration difference over a fixed distance and time, respectively, through the relationships

$$J_\alpha = \frac{-\phi D_\alpha}{\theta}\frac{dc_\alpha}{dx}, \qquad \frac{dc_\alpha}{dt} = \frac{\phi D_\alpha}{\theta}\frac{d^2c_\alpha}{dx^2} \tag{22}$$

where D_α is the species-specific diffusivity coefficient and θ is the tortuosity factor. Treatment and definition of tortuosity is variable among authors, thus it was not included in the discussion of conservation equations. This article adopts the convention whereby it is written as a constant in the denominator. In general it is a measure of the ratio of the pore connectivity length to the sediment sample length and thus its value is always greater than 1. Diffusivity of a solute ion is also temperature dependent (Robinson and Stokes, 1959). Table 1 lists a compilation of individual diffusivities (from Boudreau, 1996) for a select number of solutes as functions of temperature.

TABLE 1

Species-specific diffusivity (D) properties of select solutes

	H^+	OH^-	$SiO_{2(aq)}$	K^+	$CO_{2(aq)}$	HCO_3^-
Tc	54.4	25.9	5	9.55	5.5	5.06
Tf	1.555	1.094	0.5	0.409	0.325	0.275
D, 65 °C	0.00016	$9.7x10^{-5}$	$3.8x10^{-5}$	$3.6x10^{-5}$	$2.7x10^{-5}$	$2.3x10^{-5}$

	CO_3^-	Na^+	$Al(OH)_3$	Ca^{++}	Fe^{++}	Mg^{++}
Tc	4.33	6.06	4.46	3.6	3.31	3.43
Tf	0.199	0.297	0.243	0.179	0.15	0.144
D, 65 °C	$1.7x10^{-5}$	$2.5x10^{-5}$	$2.0x10^{-5}$	$1.5x10^{-5}$	$1.3x10^{-5}$	$1.3x10^{-5}$

Temperature (Celsius) dependence is expressed by $D = 1.0 \times 10^{-6}$ $(Tc + Tf\,T)$ (cm^2/sec). Resultant diffusivity at 65 °C are shown. The equation, and coefficients *Tc* and *Tf* that are obtained by fitting the data to the linear equation, are from Boudreau (1996).

Another fundamental process that can compete with or complement diffusive mass-transfer processes is mechanical dispersion of solutes. The effect of mechanical dispersion increases with increasing water flow velocity. Dispersion competes with chemical diffusion when the Peclet number of a system is greater than 0.4 (Bear, 1972; Ovaysi and Piri, 2011). The Peclet number of solute α for the longitudinal flow along the x axis is

$$Pe_\alpha = \frac{u_x l_c}{D_\alpha} \tag{23}$$

where u_x and l_c are flow velocity and characteristic length, respectively. The effect of dispersion can be included in the diffusion mass-transfer term by replacing the solute diffusion coefficient, D_α, with diffusion-dispersion coefficient D^*_α that also includes the effect of dispersion,

$$D^*_\alpha = D_\alpha + k_{LD} Pe_\alpha \tag{24}$$

where k_{LD} is the ratio of longitudinal dispersion to diffusion. A compilation of k_{LD}, as well as a more comprehensive review of dispersion, can be found in Ovaysi and Piri (2011), and in the references provided therein. The formalism presented herein does not account for mechanical dispersion.

Molecular diffusion of solutes with varying mobility can also produce ionic charge imbalance in the water that in turn produces electrical field difference. In response, ions of opposite charge must move in the same direction as the fast-moving ions (Robinson and Stokes, 1959). However, quantification of electrochemical potential-driven diffusivity of solutes in a multi-species solution poses a number of difficulties. Mathematically, the transport mechanism by which the ion movement can be described is not unique (Robinson and Stokes, 1959) and not trivial. Furthermore, the response of polar water molecules to the charge imbalance is also non-trivial. Therefore, this phenomenon is not addressed in the formalism presented here. As a consequence, net charge of the solution can drift away from neutral as simulations progress. As it will be shown in the second simulation example, the extent of charge imbalance that results is several orders of magnitude smaller than the ionic strengths of the interacting waters. It should also be noted that the formalism presented in this

article accurately conserves charge in closed-system cases, to the limit of the solute convergence criteria (eq 13).

WATER-ROCK INTERACTION MODEL AND APPLICATION EXAMPLES

To demonstrate the utility of the elemental mass-balance and tightly coupled mass-transfer and reaction formalism presented herein, a quantitative 1D model (acronym Sym.8) is prepared and applied to two geological water-rock interaction problems. The program is based on the sequential iteration method discussed above using a finite difference method.

In the following examples constant-temperature and constant-flux conditions were used. Given a constant-flux condition, pore water flow velocity is calculated from imposed flux using the simple relationship

$$J_{water} = \phi u \tag{25}$$

where J and u are water flux rate (volume/area-time) and its pore water velocity, respectively.

Tortuosity of sediment, used to modify the diffusion coefficient of equation (20), is assumed constant ($\theta = 3.75$) in the following simulations based on the numbers provided by Domenico and Schwarz (1998). This value is the average of tortuosities of both example cases, obtained using the Archie's equation (Archie, 1942)

$$\theta = \phi^{1-\eta} \tag{26}$$

where η is an adjustable exponent (Boudreau, 1995, 1996). The empirically fit value of the adjustable exponent reported by Boudreau (1996) is 2.14 ± 0.03. To produce the largest values of tortuosities, the exponent value of 2.17 was used to obtain tortuosities of 3.41 and 4.09 for the first (porosity 35%) and second (porosity 30%) example cases, respectively. The average of the two values is 3.75.

Porosity and surface areas of minerals for equation (6) are computed using a simple geometrical model. The model allows sediments and rocks to be described as composite porous media that follow the conservation relationship

$$\phi = 1 - \sum_{i=1}^{M} V_i \tag{27}$$

where V_i represents volume fraction of *i-th* mineral. Approximating that minerals are spherical, each can be described using two parameters, grain radii (R_γ) and number density (ρ_γ). From these total surface areas and volumes of the minerals per unit volume (/cc) of the sediment can be calculated from

$$A_\gamma = \rho_\gamma 4\pi R_\gamma^2, \qquad V_\gamma = \rho_\gamma \frac{4}{3}\pi R_\gamma^3. \tag{28}$$

Changes to grain radii from time t to $(t + dt)$ can be obtained by solving for the variable $R_{\gamma,t+\Delta t}$ in the equation

$$\Delta V_\gamma = \Delta t G_\gamma A_{\gamma,t} = \rho_\gamma \frac{4}{3}\pi (R_{\gamma,t+\Delta t}^3 - R_{\gamma,t}^3). \tag{29}$$

Permeability can be evolved with porosity and grain surface area. However, the example cases presented here are carried out using constant effluent flux conditions, which does not require permeability. Therefore, discussions on the incorporation of permeability equations into the model are not considered here.

TABLE 2

Chemical and physical properties of minerals, solutes, and reactions used in the patterned hematite precipitation example

Reactions	Log K	Kd	Vf	R
$Hematite(Fe_2O_3)_{(s)} + 2H_2O_{(l)} = 2Fe^{++}_{(aq)} + 0.5O_{2(g)} + 4OH_{(aq)}$	-65.72	$1.8x10^{-18}$	0	0
$Quartz(SiO_2)_{(s)} = SiO_{2(aq)}$	-3.427	Non-reactive; set to zero	0.65	0.04
$H_2O_{(l)} = H^+_{(aq)} + OH_{(aq)}$	-12.95	--	--	--

Log K: $\log_{10}$ of equilibrium constant; kd: dissolution rate constant at 64 °C, mol/cm^2-sec; Vf: volume fraction; R: grain radii, cm. Vf and R are at the starting conditions at the beginning of simulations. Log K from EQ3/6 database, Wolery and others, (1990); Ea and kd from Palandri and Kharaka (2004)

Water composition (Molar)				Domain setup
Solute	Formation water	Water in fracture	Solute diffusivity[1]	5 meter long quartzose sandstone. Left boundary at fracture surface. Water influx from left at variable rates. 500 finite difference grid points. Isothermal, 64 °C
H^+	$2.1x10^{-7}$	$1.0x10^{-6}$	$4.1x10^{-5}$	
Fe^{++}	$4.0x10^{-18}$	$6.6x10^{-14}$	$3.4x10^{-6}$	
$O_{2(g)}$	$1.0x10^{-8}$	$5.0x10^{-14}$	$5.5x10^{-6}$	

[1] Solute diffusivities shown are tortuosity-adjusted solute diffusion coefficients.

Na (number of solute species)	Ne[2] (number of chemical elements)	Nf (fast equilibrium reactions)	Total number of equations (Ne + Nf)
6 (Fe^{++}, $O_{2(g)}$, H_2O, OH^-, H^+, $SiO_{2(aq)}$)	5 (Fe, O_2, O, H, Si)	1 (water)	6

[2] O_2 is used as a pseudo-element to simplify the Fe redox (hematite) reaction.

Iron-oxide Precipitation in a Diffusive-Reaction System

Iron-oxide concretions and nodules are common features in Lower Jurassic Navajo Sandstone of southern Utah (Chan and others, 2000). Based on extensive field work and simple mass-balance calculations, Chan and others (2000) hypothesized that the iron was sourced from trace amounts of iron-oxide coating the sand grains and that the iron was liberated when it was exposed to reducing fluids moving upward from deeper reservoirs. Numerical simulations using the methodology presented here, along with laboratory experiment results, were presented in Chan and others (2007) in support of the proposed hypothesis. This geologic example is used herein with different boundary conditions and domain configuration than those presented in the Chan and others (2007).

The set up of the simulations is shown in table 2. The domain is a five-meter long sandstone consisting only of clean quartz grains of uniform spherical size. The chemical system is described by four elements (Si, Fe, O, and H). The fifth pseudo-element, O_2, was added to the system to simplify the redox process described by the hematite dissolution reaction (table 2), which is produced by combining

$$Fe_2O_{3(s)} + 6H^+_{(aq)} = 2Fe^{+++}_{(aq)} + 3H_2O_{(l)} \qquad (30)$$

and

$$Fe^{+++}_{(aq)} + 0.5H_2O_{(l)} = Fe^{++}_{(aq)} + H^{+}_{(aq)} + 0.25O_{2(g)}. \quad (31)$$

This simplification approach allows the solutes Fe^{+++} and $O_{2(g)}$ to be excluded from the chemical system. Thus, by introducing a pseudo-element O_2 that represents $O_{2(aq)}$, the chemical reaction network has been made simpler, the immediate benefit of which is the reduced stiffness of the Jacobian matrix (see eq 13), and therefore reduced the computation time required to carry out the simulation.

No hematite is present at the beginning of the simulation. The water in the fracture is slightly below equilibrium with respect to hematite at water pH 5.0, whereas the resident water is slightly below equilibrium with respect to hematite at an oxygen level of 1×10^{-8} M and water pH of 6.8. The difference in the water pH values results in higher Fe^{++} concentration along the fracture than that in the resident water. Thus, the left and right boundaries are subjected to waters enriched in Fe^{++} and $O_{2(g)}$, respectively. Iron-oxide precipitation occurs when Fe^{++} infiltrates into sandstone and interacts with the oxygen-rich resident water.

A series of simulations were performed with varying water fluxes to produce water flow velocities of 0.0 up to 100 cm per year. To simulate a nucleation barrier (threshold), hematite nucleation is assumed to occur when the saturation state of hematite is 50 percent above equilibrium saturation. When this nucleation threshold is exceeded, a fixed number per unit volume (number density) of hematite nucleates. The number density used in the simulations is 3.5×10^{5} grains/cc, an approximation based on the number of fine sand grains in a unit volume of sandstone. The nucleating grain radius is set at 3.5×10^{-8} cm, which approximates the size of a cluster of hematite crystals whose unit volume is 302 $Å^3$ (Deer, and others, 1966).

Figure 2 shows the evolution of nucleation sites as a function of time. In this and subsequent figures, the saturation of water with respect to hematite is used to indicate the state of water reactivity. Once the nucleation threshold value is achieved at any point in the sandstone, there is a rapid depletion of solute from water at that point. This is accompanied by diffusive influx of solutes from the immediate surroundings, resulting in reduced reactant concentrations and mineral saturation adjacent to the nucleated hematite.

In the simulation shown in figure 2, the first cluster of precipitation forms along the fracture boundary due to the high saturation achieved when the Fe-enriched water enters the sandstone. The immediate consequence of hematite precipitation along the margin is the depletion of oxygen in the sand, as shown in figure 3, and decreased hematite saturation (fig. 2). Continued diffusive influx results in increased saturation until the second nucleation occurs (up-arrow, fig. 2). This process continues until a series of nucleations occur away from the fracture margin. Simulations were run for short time periods (10's to 100's of years) due to extremely small timesteps (in the order of seconds to minutes per iteration). Volume fraction of iron oxide nodules precipitating during the simulation period is far less than 1 percent, thus not included in the results shown.

Diffusion alone can supply only a limited quantity of Fe through the fracture surface. However, it is also plausible that advective infiltration of water into the sandstone would be occurring when water is flowing in the fracture network, which would result in a greater quantity of solutes entering the sandstone. The consequence is that nucleate distribution pattern changes significantly with varied advective infiltration rate (fig. 4). As water flow velocity increases, a greater number of nucleation sites form further into the sandstone. Figure 4D shows that water flow velocity of 100 cm/year is insufficient to counter the diffusive infiltration of oxygen from the right boundary. High rate of diffusion results from the combination of the species-specific diffusivity coefficient and the chemical potential gradient prevailing between right and left boundaries. As a result, hematite precipitation continues unabated throughout the

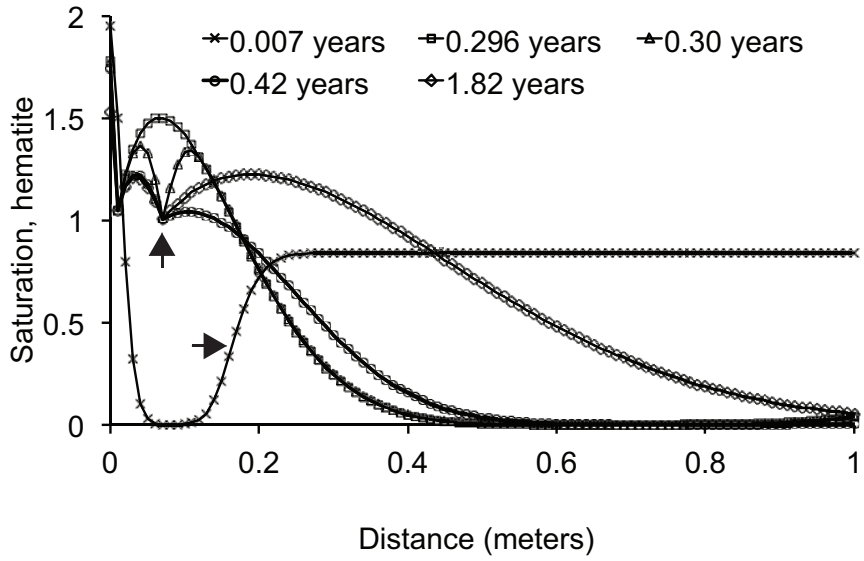

Fig. 2. Saturation patterns within the first meter of a 5 meter-long simulation domain at five different simulation times. In this simulation, water rich in Fe^{++} and depleted in $O_{2(g)}$ is entering the sediment from the left by diffusion only. The suppressed saturation level propagating inward (right-arrow) is due to diffusive depletion of oxygen (see fig. 3B). First precipitation of hematite at the left boundary occurs instantaneously when the water enters the sediment. Second precipitation at 0.08 meters (up-arrow) occurs between 0.296 and 0.3 years, after the saturation has reached the nucleation thresh-hold of 1.5 (50% above saturation). Drop in the saturation from 1.5 to 1 is a result of rapid hematite precipitation, which also depletes Fe^{++} and $O_{2(g)}$ from water in neighboring sediments and suppresses hematite precipitation there.

sandstone even as the nucleation precipitation front advances inward. Predictably, with increasing water flux and therefore quantity of Fe imported, an increasing number of nucleation sites is produced.

Ultimately, the hematite nucleation and distribution pattern depends on diffusive and advective mass-transfer processes that supply the solutes, and the reaction mechanisms that consume the solutes. While the advection rate is an imposed condition, reaction and diffusion rates are interdependent (nonlinear) processes that can modify each other's behaviors. In effect, the formalism presented successfully captures the nonlinear competition between the rate of supply and the rate of consumption of solutes, and the ensuing self-organizing process. While the theoretical model for a similar reaction-diffusion was proposed earlier (Ortoleva and others, 1987; Ortoleva, 1994), the formalism and the field application presented here and in Chan and others (2007) are the most comprehensive to date.

Interaction of CO_2-charged and Formation Waters in a Saline Reservoir

The second example simulates the interaction between CO_2-rich water evolved from the mix of CO_2 injected into a siliciclastic saline reservoir, and the resident formation water. This example involves a greater number of solutes (16) than the first example. It addresses the types of water-rock interactions that may occur during carbon sequestration in geologic formations. While field applications call for multi-dimensional multi-phase fluid flow and heat transfer modeling, this example simulation focuses on the interaction of CO_2-rich water and the resident sediment far from the injection port, beyond the region where supercritical and liquid CO_2 phases dominate. It is intended to characterize the response of siliciclastic minerals to changing water pH induced by the injected carbon.

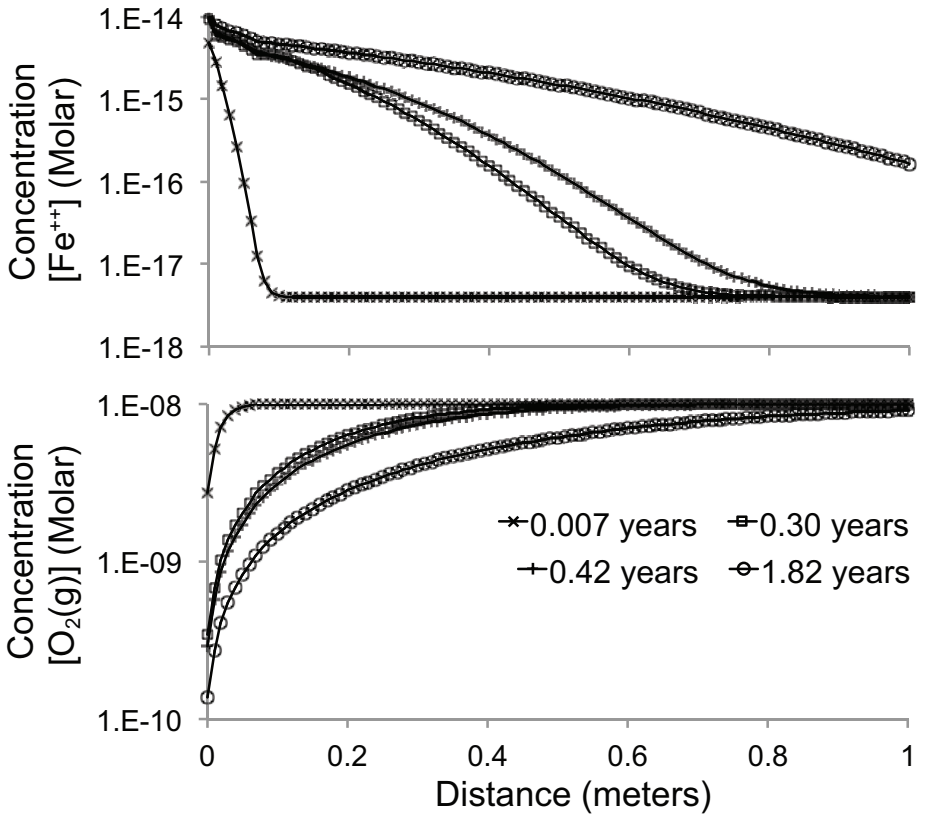

Fig. 3. Concentration profiles of Fe^{++} (A) and $O_{2(g)}$ (B) at four simulation times show diffusive infiltration of Fe^{++} into the sediment and progressive depletion of $O_{2(g)}$ with time. Precipitation of hematite at two nucleation points are insufficient to deplete all available Fe^{++}, implying that diffusive mass transfer rate is greater than precipitation rate. Oxygen abundance is orders of magnitude greater than that of iron, thus hematite precipitation is limited by availability of Fe^{++}.

This simulation example is loosely based on published information from the South Liberty oil field injection pilot study in the Frio Formation, Gulf of Mexico (Kharaka and others, 2006). As shown in table 3, a 50 meter-long segment of a reservoir is subjected to effluent flow rate of 100 meters per year and six minerals characterize the sediment. The resident pore water before the injection is based on the typical composition of known Gulf of Mexico sandstones (Land and Macpherson, 1992). The effluent is the same water but with higher alkalinity to mimic the CO_2 charging that results from the interaction of CO_2 and the formation water closer to the CO_2 injection port. To track the location of the sweep front (interface where CO_2-rich effluent is displacing formation water), the Fe^{++} concentration of the effluent (a solute not partaking in any reaction) is set at a higher value than that of the formation water. The configuration and duration of the numerical experiments are not precisely comparable to the field test results reported by Kharaka and others (2006). Nonetheless, the numerical simulation results do show geochemical traits that are consistent with the field observations.

The result of the simulation at 0.25 years of simulated time is shown in figure 5. All of the solutes shown, in particular H^+ and bicarbonates, produce complex patterns across the sweep front. This phenomenon is associated not only with the water-rock

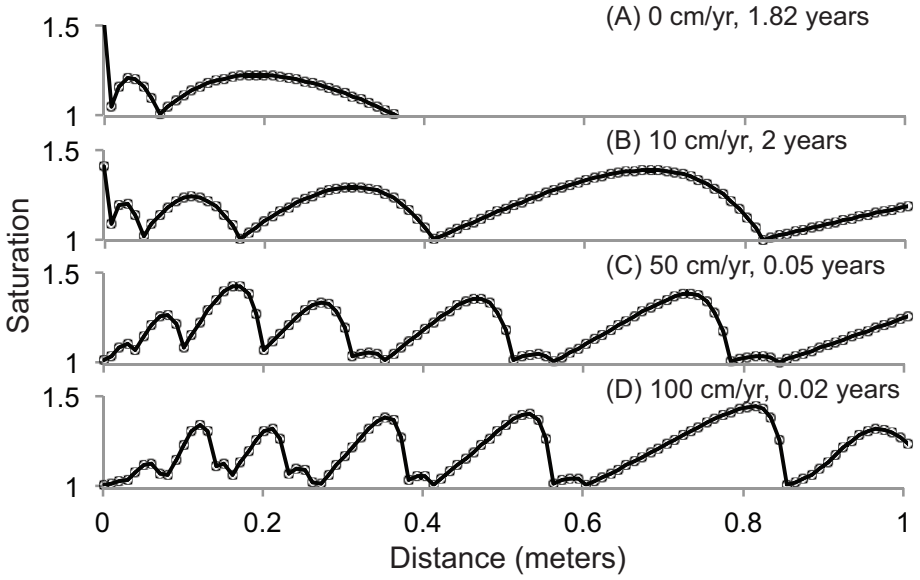

Fig. 4. Hematite saturation patterns within the first meter of a 5 meter-long simulation domain at four different fluid flow rates. In these simulations, water rich in Fe^{++} and depleted in $O_{2(g)}$ is advecting into the sediment from the left. Increasing advective infiltration rate of Fe-rich water results in progressively greater quantity of hematite precipitating and the formation of precipitation patterns. (A) In diffusion-only system only a limited precipitation pattern emerges as diffusion alone can only provide a limited quantity of Fe^{++}. (B) A regularly periodic pattern emerges at a moderate infiltration rate. (C), (D) Complex patterns emerge at higher infiltration rates, and eventually result in hematite precipitating throughout the sediment within first 0.2 years. Even at a 1 meter/year flow rate, oxygen is able to diffuse upstream and produce hematite precipitates throughout the sediment.

interaction immediately behind the sweep front, but also due to diffusive mobility of the solutes. Thus, as the CO_2-rich water is displacing and mixing with the formation water, a series of complex diffusion and reaction fronts are forming in the vicinity of the sweep front (fig. 5A).

In figure 5B saturations of minerals are shown. The general trend is for all feldspars to become strongly undersaturated in the acidic water behind the sweep front, the immediate effect of which is to make the water extremely highly saturated with respect to kaolinite. The low pH of the water also suppresses calcite saturation behind the sweep front, even as additional Ca is released from the dissolving feldspars. Saturation is used to indicate the reactivity of minerals instead of mineralization rates, since the latter can change depending on available reactive surface area.

As discussed earlier, the solution ionic charge can drift from the neutral as solutes move with varying diffusivities. Figure 5C is a profile of net charge across the simulation domain. The inlet and formation waters have zero net charges that were achieved by adjusting concentrations of Cl^- (table 3). The zone of charge imbalance occurs as different solutes migrate at different rates, according to their unique diffusive properties and concentration gradients. The net charge imbalance occurring is therefore the combined effect of all solutes involved. Considering the higher diffusivity property of Cl^-, and its concentration that is higher by at least two orders of magnitude than other solutes, and the abundance of Cl^- in natural waters, the charge imbalance can be addressed primarily by including a simple electrochemical mobilization term to the diffusivity of Cl^-.

TABLE 3

Chemical and physical properties used in the example of CO_2-charged water and formation water interaction

Reactions	Log K	kd	Vf	R
$Quartz(SiO_2)_{(s)} = SiO_{2(aq)}$	-3.16	$7.3x10^{-17}$	0.46	0.002
$K\ feldspar\ \left(K_{0.5}Na_{0.5}AlSi_3O_8\right)_{(s)} + 2H_2O_{(l)} =$ $0.5K^+_{(aq)} + 0.5Na^+_{(aq)} + OH_{(aq)} + Al(OH)_{3(aq)} + 3SiO_{2(aq)}$	-24.35	$1.5x10^{-17}$	0.10	0.003
$Plagioclase\ \left(Ca_{0.38}Na_{0.62}Al_{1.38}Si_{2.62}O_8\right)_{(s)} + 2.76H_2O_{(l)} = 0.38Ca^{++}_{(aq)}$ $+0.62Na^+_{(aq)} + 1.38OH_{(aq)} + 1.38Al(OH)_{3(aq)} + 2.62SiO_{2(aq)}$	-26.22	$1.3x10^{-16}$	0.10	0.003
$Albite\ \left(NaAlSi_3O_8\right)_{(s)} + 2H_2O_{(l)} =$ $Na^+_{(aq)} + OH_{(aq)} + Al(OH)_{3(aq)} + 3SiO_{2(aq)}$	-23.26	$1.3x10^{-17}$	0.02	0.003
$Calcite\ \left(CaCO_3\right)_{(s)} = Ca^{++}_{(aq)} + CO_{3(aq)}$	-9.17	$7.0x10^{-13}$	0.015	0.0001
$Kaolinite\left(Al_2Si_2O_5\left(OH\right)_4\right)_{(s)} + H_2O_{(l)} =$ $2Al(OH)_{3(aq)} + 2SiO_{2(aq)}$	-21.15	$2.9x10^{-19}$	0.005	0.00001
$Illite\left(KAl_3Si_3O_{10}\left(OH\right)_2\right)_{(s)} + 4H_2O_{(l)} =$ $K^+_{(aq)} + OH_{(aq)} + 3Al(OH)_{3(aq)} + 3SiO_{2(aq)}$	-41.31	$9.0x10^{-19}$	0.0	0.0
$H_2O_{(l)} = H^+_{(aq)} + OH_{(aq)}$	-12.95	--	--	--
$H^+_{(aq)} + CO_{(aq)} = HCO_{3(aq)}$	10.08	--	--	--
$CO_{2(aq)} + H_2O_{(l)} \quad H^+_{(aq)} + HCO_{(aq)}^-$	-6.344	--	--	--

See Table 2 for explanations and units of the variables. Mineral reactions are for neutral pH range. Log K from EQ3/6 database, Wolery and others (1990); kd at 90 °C are calibrated data based on Palandri and Kharaka (2004) and other sources referenced therein.

Solute	Water composition (Molar)		Diffusivity[1]	
	Formation	CO_2-rich	(cm^2/sec)	
H^+	$2.57x10^{-6}$	$1.0x10^{-4}$	$5.2x10^{-5}$	50 meters long (sandstone reservoir), starting porosity 30% 200 finite difference grids filled with formation water subjected to constant influx of CO_2-rich water from left boundary Water flow velocity 100 meters/year Isothermal, 90 °C
$CO_{2(aq)}$	Total 0.002	Total 0.5	$2.1x10^{-5}$	
HCO_3^-			$7.9x10^{-6}$	
CO_3^{--}			$5.9x10^{-6}$	
Ca^{++}	0.0025	0.0025	$5.3x10^{-6}$	
$Al(OH)_3$	$1.7x10^{-6}$	$1.7x10^{-6}$	$7.0x10^{-6}$	
K^+	0.00005	0.00005	$1.2x10^{-5}$	
$SiO_{2(aq)}$	0.001	0.001	$1.3x10^{-5}$	
Na^+	0.4	0.4	$8.7x10^{-6}$	
Cl^-	0.4035	0.4035	$1.3x10^{-5}$	
Fe^{++}	$1.0x10^{-6}$	$5.0x10^{-6}$	$4.5x10^{-6}$	
Mg^{++}	$1.0x10^{-5}$	$5.0x10^{-5}$	$4.4x10^{-6}$	

[1] Solute diffusivities shown are tortuosity-adjusted solute diffusion coefficients.

Na (number of solute species)	Ne (number of chemical elements)	Nf (fast equilibrium reactions)	total number of equations (Ne + Nf)
14 (solutes listed above + OH^-, H_2O)	11 (Ca, K, Na, Al, Si, Fe, Mg, Cl, Ca, H, O)	3 (water + 2 bicarb complexations)	14

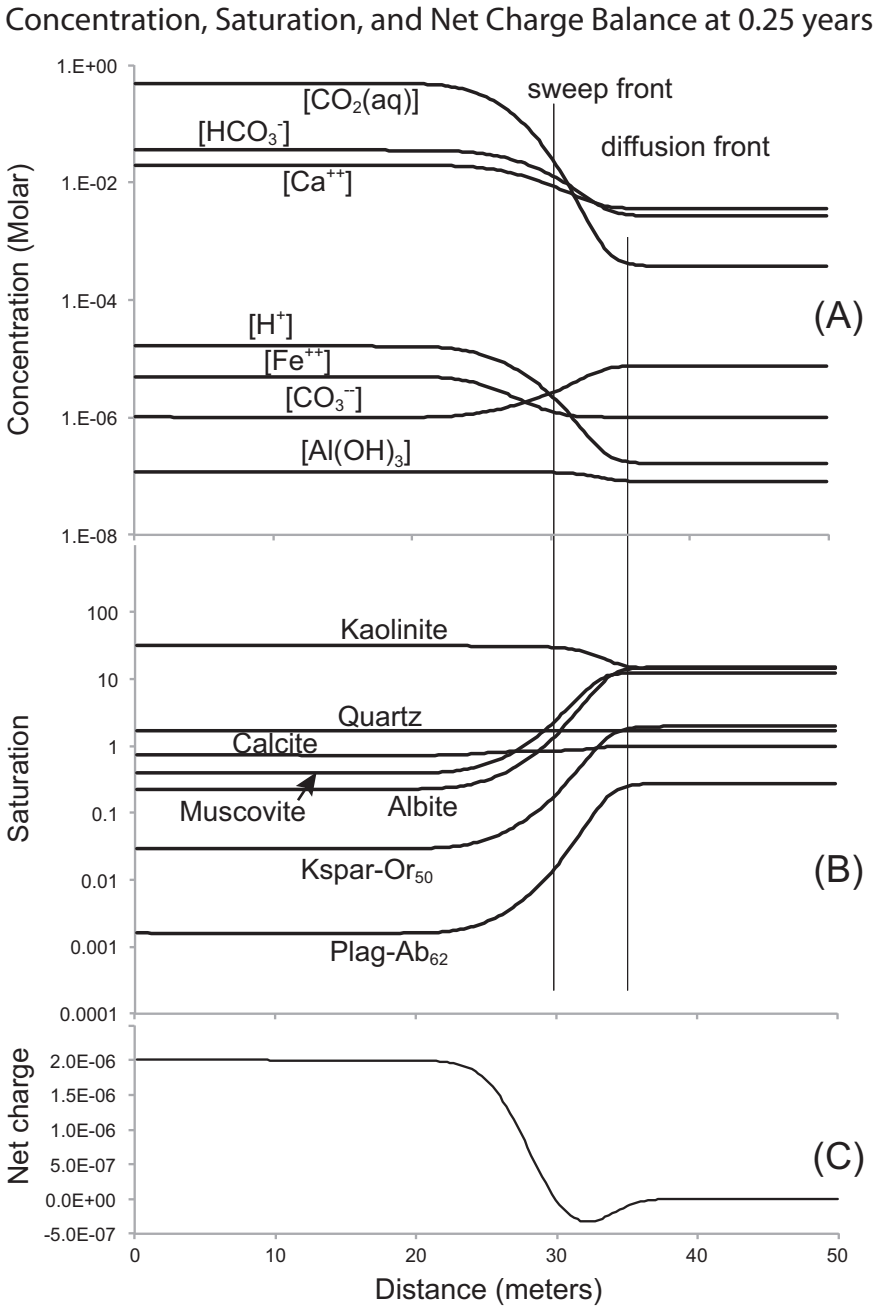

Fig. 5. Concentration profiles of select species (A), mineral saturations (B), and net ionic solution charge balance (C) at a simulation time of 0.25 years show complex reaction front develops when CO_2-rich water is forced into a sandstone reservoir. Effluent flow rate (pore velocity) of 10 meters/year is imposed. (A) Sweep front marks where CO_2-rich effluent is displacing formation water, and is identified by a shift in Fe^{++} concentrations at around the 30 meter mark. Displaced H^+ and bicarbonates ahead of the sweep front is due to diffusive flux of H^+ exceeding the rate of effluent flow rate; bicarbonate species variation is due to complexation reactions. For brevity, concentrations of Na^+, K^+, and $SiO_{2(aq)}$ are excluded, since they show negligible changes across the simulation domain. (B) Under low acidic condition produced by high CO_2 concentration, all feldspars, calcite, and illite become highly undersaturated (saturation < 1), resulting in supersaturation of quartz and kaolinite (saturation > 1). (C) Differences in solute diffusion properties result in variable ionic charge of the solution where the two waters interact. The resulting net charge discrepancy is orders of magnitude smaller than concentrations of most dominant solutes, Na^+ and Cl^-.

The evolution of a diffusion front ahead of the sweep front provides an insight into the findings from the Frio Formation CO_2 field test. Kharaka and others (2006) indicates that when CO_2 was injected into the formation, the monitoring well showed increased acidity and bicarbonate prior to the arrival of the CO_2 sweep front. Furthermore, the Frio Formation test suggested an increase in concentrations of cations not typically associated with sandstones (such as Fe and Mn), suggesting that the acidic water may have interacted with shales (Kharaka and others, 2006). This observation is consistent with the expectation that a significant quantity of solutes, in particular H^+, may have infiltrated diffusively into the shale to cause enhanced clay reactions. A similar trend of water pH and alkalinity shift before the arrival of the CO_2 front has been observed elsewhere (Takacs and others, 2011).

The diffusion front that forms in advance of the sweep front is transient, thus it may be of minor importance to the reservoir integrity. However, it is possible that the reduced pH and higher bicarbonate concentrations within the diffusion zone may have an important implication on mineral surface wetting properties as well as surface tensions of residual oil and imbibed CO_2 liquid and/or supercritical phase droplets. Sufficient evidence in favor or to the contrary of this conjecture is lacking in the literature, even as pH and other solute's effect on oil and gas droplet behaviors have been documented (Carre and Lacarriere, 2006; Espinoza and Santamarina, 2010).

DISCUSSION

The water-rock interaction and reactive-transport methodology presented herein uses elemental mass conservation equation and tight coupling between mass-transfer and reaction terms of the conservation equation. The approach contrasts with the conventional method of solving solute species mass-conservation equations using loosely coupled mass-transfer and reaction processes. The two examples provided show the extent of the methodology's utility. The simulator can model extremely fast redox-type reactions as well as engineering and geologic time-scale problems. This flexibility is achieved by implementing only the first-principle expressions of the conservation equation and associated processes in the simulator.

Capturing the nonlinear feedback between fluid flow and sediment heterogeneity requires a carefully designed and implemented textural model. For human time-scale problems that do not involve extensive sediment textural and compositional alteration an accurate heterogeneity model with accurate porosity-permeability description may provide sufficient feedback between flow and sediment heterogeneity. For problems of geologic time scale, or those involving extensive alteration to sediment composition and texture, the textural model must be able to provide sufficiently accurate textural alteration feedback that is consistent with the extent of mass-changes dictated by the water-rock interaction model. Since there is no theoretical means to determine the accuracy of a textural model, it can only be achieved by calibrating the model with observable geologic or experimental data. The examples shown in this paper did not require an elaborate texture model, since insignificant textural modifications were observed within the simulation period. A more comprehensive example will be given in the follow-up paper to this one that describes two-dimensional pattern formation associated with total dolomitization of shallow-buried limestones.

CONCLUSION

Existing continuum-based water-rock interaction models solve solute conservation equations. An alternative methodology is presented that uses elemental mass conservation equations. Other important differences between the existing and the proposed methodology include the solute-specific diffusivity and clearly defined tight coupling between mass-transfer and reaction terms of the conservation equations. The pro-

posed model also achieves greater clarity and simplicity over existing methodologies on how the systems of equations are constructed.

The utility of the methodology is demonstrated by two simulation examples, one involving a redox-type hematite precipitation in a diffusion-reaction system, and the other involving an engineering-time scale problem of injecting CO_2-rich effluent into a saline reservoir. In both examples diffusive mass-transfers are found to be important facets for inducing patterns or dissipating reactive solutes.

ACKNOWLEDGMENTS

Maintenance and development of the work presented was made possible in part by the sponsors of the AVID carbonate diagenesis (University of Colorado, Boulder) and Balance clastic diagenesis (Sienna Geodynamics and Consulting, Inc.) consortiums: BG Group, Chevron, ConocoPhilips, ExxonMobil, and Shell. The author wishes to thank Yifeng Wang and two other anonymous reviewers for their critical and constructive comments, which contributed significantly to improving the quality of this manuscript. David A. Budd (University of Colorado, Boulder) provided many critical discussions, as well as feedbacks on early drafts and revisions.

Rerefences

Archie, G. E., 1942, The electrical resistivity log as an aid in determining some reservoir characteristics: Transactions of the AIME, v. 146, n. 1, p. 54–62.

Atkinson, K., 1988, An introduction to numerical analysis: New York, John Wiley & Sons, 693 p.

Bear, J., 1972, Dynamics of fluids in porous media: New York, Dover Publications, Inc., 764 p.

Boudreau, B., 1995, The diffusive tortuosity of fine-grained unlithified sediments: Geochimica et Cosmochimica Acta, v. 60, n. 16, p. 3139–3142, http://dx.doi.org/10.1016/0016-7037(96)00158-5

——— 1996, Diagenetic models and their implementation: New York, Springer, 414 p.

Carre, A., and Lacarriere, V., 2006, Study of surface charge properties of minerals and surface-modified substrates by wettability measurements: Contact Angle, Wettability and Adhesion, v. 4, p. 1–14.

Chan, M. A., Parry, W. T., and Bowman, J. R., 2000, Diagenetic hematite and manganese oxides and fault-related fluid flow in Jurassic sandstones, southeastern Utah: American Association of Petroleum Geologists Bulletin, v. 84, n. 9, p. 1281–1310, http://dx.doi.org/10.1306/A9673E82-1738-11D7-8645000102C1865D

Chan, M. A., Ormo, J., Park, A., Stich, M., Souza-Egipsy, V. S., and Komatsu, G., 2007, Models of iron oxide concretion formation: field, numerical, and laboratory comparisons: Geofluids, v. 7, n. 3, p. 356–368, http://dx.doi.org/10.1111/j.1468-8123.2007.00187.x

Courant, R., Friedrichs, K., and Lewy, H., 1928, On the partial difference equations of mathematical physics: Mathematische Annalen (in German), v. 100, n. 1, p. 32–74, http://dx.doi.org/10.1007/BF01448839. Reprinted in 1967: Courant, R., Friedrichs, K., and Lewy, H., 1967, On the partial difference equations of mathematical physics: IBM Journal of Research and Development, v. 11, n. 2, March, p. 215–234.

Deer, W. A., Howie, R. A., and Zussman, J., 1966, An introduction to the rock-forming Minerals: London, Longman, 528 p.

DeGroot, A., and Mazur, P., 1962, Non-equilibrium thermodynamics: Amsterdam, North-Holland Publishing Co., 510 p.

Domenico, P., and Schwartz, F., 1998, Physical and chemical hydrogeology, 2nd edition: New York, John Wiley & Sons, 506 p.

Espinoza, D. N., and Santamarina, J. C., 2010, Water-CO_2-mineral systems: interfacial tension, contact angle, and diffusion—implications to CO_2 geological storage: Water Resources Research, v. 46, n. 7, W07534, http://dx.doi.org/10.1029/2009WR008634

Eyring, H., 1935, The activated complex in chemical reactions: The Journal of Chemical Physics, v. 3, n. 107, p. 107–115, http://dx.doi.org/10.1063/1.1749604

Kharaka, Y. K., Cole, D. R., Hovorka, S. D., Gunter, W. D., Knauss, K. G., and Freifeld, B. M., 2006, Gas-water-rock interactions in Frio Formation following CO_2 injection: Implications for the storage of greenhouse gases in sedimentary basins: Geology, v. 34, n. 7, p. 577–580, http://dx.doi.org/10.1130/G22357.1

Kirkner, D. J., and Reeves, H., 1988, Multicomponent mass transport with homogeneous and heterogeneous chemical reactions: Effect of the chemistry on the choice of numerical algorithm 1. Theory: Water Resources Research, v. 24, n. 1, p. 1719–1729, http://dx.doi.org/10.1029/WR024i010p01719

Land, L. S., and Macpherson, G. L., 1992, Geothermometry from brine analyses: lessons from the Gulf Coast, U.S.A.: Applied Geochemistry, v. 7, n. 4, p. 333–340, http://dx.doi.org/10.1016/0883-2927(92)90023-V

Lichtner, P., 1985, Continuum model for simultaneous chemical reactions and mass transport in hydrothermal systems: Geochimica Cosmochimica Acta, v. 49, n. 3, p. 779–800, http://dx.doi.org/10.1016/0016-7037(85)90172-3

Millero, F. J., 1971, The molal volumes of electrolytes: Chemical Reviews, v. 71, n. 2, p. 147–176, http://dx.doi.org/10.1021/cr60270a001

Ortoleva, P., 1994, Geochemical self-organization: New York, Oxford University Press, 411 p.
Ortoleva, P., Merino, E., Moore, C., and Chadam, J., 1987, Geochemical self-organization I: Reaction-transport feedbacks and modeling approach: American Journal of Science v. 287, n. 10, p. 979–1007, http://dx.doi.org/10.2475/ajs.287.10.979
Ovaysi, S., and Piri, M., 2011, Pore-scale modeling of dispersion in disordered porous media: Journal of Contaminant Hydrology, v. 124, n. 1–4, p. 68–81, http://dx.doi.org/10.1016/j.jconhyd.2011.02.004
Palandri, J. L., and Kharaka, Y. K., 2004, A compilation of rate parameters of water-mineral interaction kinetics for application to geochemical modeling: USGS Open File Report 2004-1068, 64 p.
Park, A., and Ortoleva, P., 2003, WRIS.TEQ: multi-mineralic water-rock interaction, mass-transfer and textural dynamics simulator: Computers and Geosciences, v. 29, p. 277–290, http://dx.doi.org/10.1016/S0098-3004(03)00005-0
Parkhurst, D., Thorstensen, D., and Plummer, L., 1980, PHREEQE—A computer program for geochemical calculations: U.S. Geological Survey Water Resources Investigation 80-96, 193 p.
Perkins, E. H., Kharaka, Y. K., Gunter, W. D., and DeBraal, J. D., 1988, Geochemical modeling of water-rock interactions using SOLMINEQ.88, *in* Melchior, C., and Basset, R. L., editors, Chemical Modeling of Aqueous Systems II D., Symposium Series 416: Washington, D.C., American Chemical Society National Meeting 196, p. GEOC 25.
Press, W. H., Flannery, B. P., Teukolsky, S. A., and Vetterling, W. T., 1992, Numerical Recipes in C: The Art of Scientific Computing, 2nd edition: Cambridge, Cambridge University Press, 994 p.
Raffensperger, J. P., and Garven, G., 1995, The formation of unconformity-type uranium ore deposits, 1. Coupled groundwater flow and heat transport modeling: American Journal of Science, v. 295, n. 5, p. 581–636, http://dx.doi.org/10.2475/ajs.295.5.581
Robinson, R. A., and Stokes, R. H., 1959, Electrolyte Solutions: London, United Kingdom, Butterworth & Co., 559 p.
Rubin, J., 1983, Transport of reacting solutes in porous media: Relation between mathematical nature of problem formulation and chemical nature of reactions: Water Resources Research, v. 19, n. 5, p. 1231–1252, http://dx.doi.org/10.1029/WR019i005p01231
Steefel, C. I., and Lasaga, A. C., 1994, A coupled model for transport of multiple chemical species and kinetic precipitation/dissolution reactions with application to reactive flow in single phase hydrothermal systems: American Journal of Science, v. 294, n. 5, p. 529–592, http://dx.doi.org/10.2475/ajs.294.5.529
Takacs, K., Beck, E., Parris, T., Wedding, D., and Locke, R., 2011, Aqueous geochemistry of a carbon dioxide-enhanced oil recovery project in the Sugar Creek oil field, western Kentucky: Washington, D.C., September 25–27, 2011, American Association of Petroleum Geologist Eastern Section 40th Annual Meeting Abstracts with Programs, p. 52.
Truesdell, A. H., and Jones, B. F., 1974, WATEQ, a computer program for calculating chemical equilibria of natural waters: Reston, Virginia, USGS, USGS PB-220464, 77 p.
White, A., and Chuma, N., 1986, An EQ3/EQ6 reaction path model of chemical evolution in the Valles hydrothermal system, New Mexico, USA, *in* Hitchon, B., editor, Fifth International symposium on Water-rock Interaction: Reykjavik, Iceland. Proceedings of 5th International Symposium on Water-Rock Interaction, p. 626–628.
Wolery, T. J., 1992, EQ3NR, a computer program for geochemical aqueous speciation-solubility calculations: Theoretical manual, User's guide, and related documentation (version 7.0), UCRL-MA-110662 PT III: Livermore, California, University of California, 262 p.
Wolery, T. J., Jackson, K. J., Bourcier, W. L., Bruton, C. J., Viani, C., Knauss, K. G., and Delany, J. M., 1990, Current status of the EQ3/6 software package for geochemical modeling, *in* Melchior, D. C., and Bassett, R., editors, Chemical Modeling of Aqueous Systems II: Washington, D.C., American Chemical Society Symposium Series 416, American Chemical Society, p. 104–116.
Xu, T., and Pruess, K., 2001, Modeling multiphase non-isothermal fluid flow and reactive geochemical transport in variably saturated fractured rocks: 1. Methodology: American Journal of Science, v. 301, n. 1, p. 16–33, http://dx.doi.org/10.2475/ajs.301.1.16
Yeh, G., and Tripathi, V. S., 1991, A model for simulating transport of reactive multispecies components: Model development and demonstration: Water Resources Research, v. 27, n. 12, p. 3075–3094, http://dx.doi.org/10.1029/91WR02028